ORIGINAL PAPER

Sub-surface geometry of Ar Rika and Ruwah faults from gravity and magnetic surveys

S. Mogren · A. M. Al-Amri · K. Al-Damegh ·
D. Fairhead · S. Jassim · A. Algamdi

Abstract Ten global positioning system (GPS)–gravity profiles were conducted to provide sub-surface geometry of two sections of the Najd Fault System (NFS) Ruwah and Ar Rika faults, six in the Afif and four in the Al Muwayh area about 500 and 650 km west of Riyadh, respectively. GPS surveys were collected in differential GPS (DGPS) mode, allowing a large area to be covered in limited time. DGPS is utilized for the advantages of accuracy, economy, and speed. Output DGPS location coordinates were used in free-air and Bouguer reductions; terrain corrections were applied using a 3-arcsecond digital elevation model; finally, isostatic and decompensative corrections were applied. Integration of the resulting decompensative isostatic residual anomalies and aeromagnetic map has mapped the NFS very accurately. Modeling the gravity field crossing the Ruwah fault zone revealed that it is associated with low gravity anomalies probably due to a complex of lower density crushed rocks and modeled the geometry of the subsurface structure of Ar Rika fault as an inclined fault with reverse movement that would imply a compression component (post-dated the shearing) parallel to the plane of the cross-section.
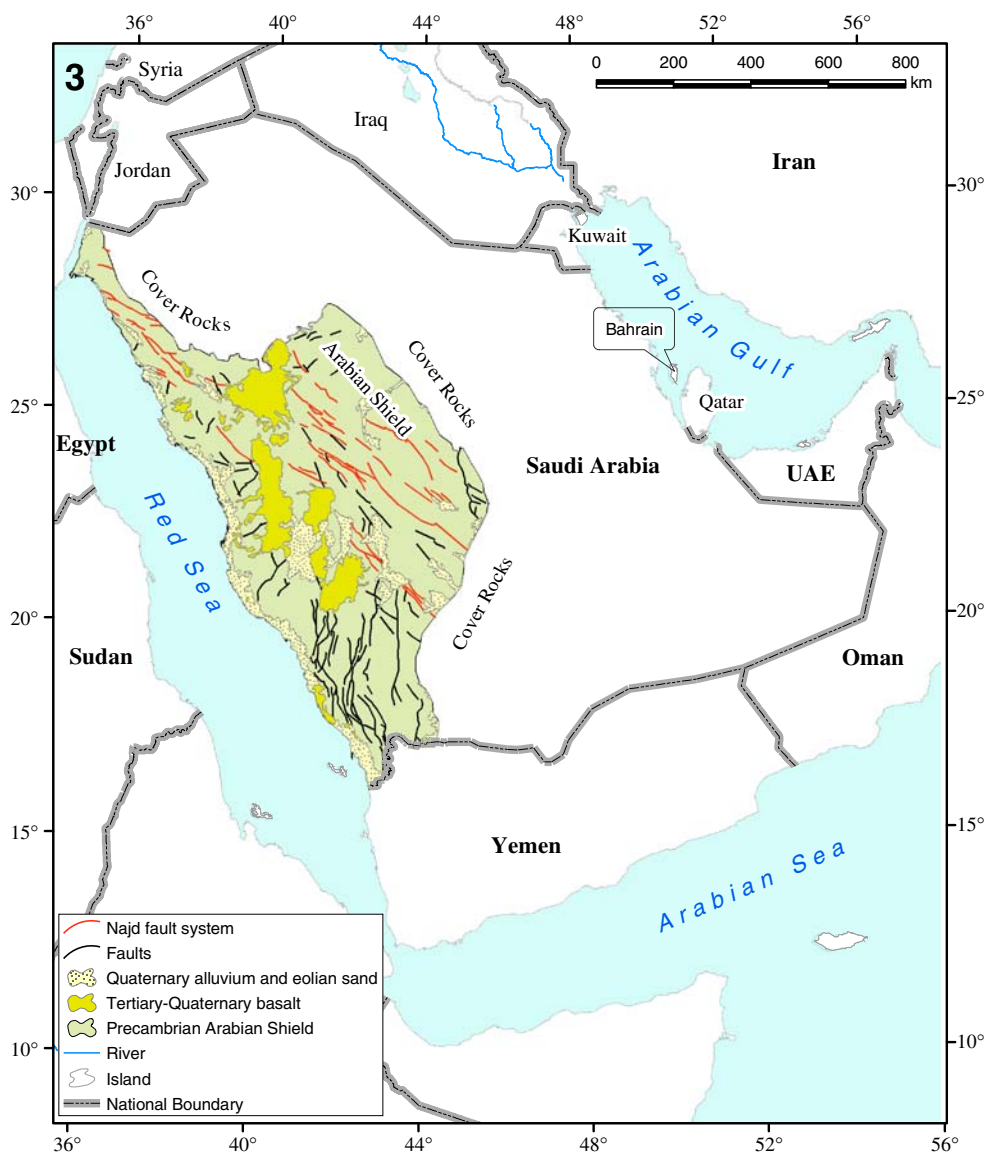
S. Mogren (✉) · A. M. Al-Amri
Geology Department, College of Sciences, King Saud University,
Riyadh, Saudi Arabia
e-mail: s_mogren@yahoo.com

K. Al-Damegh · A. Algamdi
King Abdulaziz City for Science and Technology,
Riyadh, Saudi Arabia

D. Fairhead
Earth Sciences Department, University of Leeds,
Leeds, England

S. Jassim
GETECH,
Leeds, England

Introduction

Ruwah and Ar Rika faults are part of the Najd fault system (NFS), which is one of the most prominent structural features in the Arabian Shield (Fig. 1). It is a system of primary and secondary strike–slip faults, crossing the Arabian Shield from NW to SE and severely disrupting the amalgamated Shield terranes. It is one of the largest recognized Proterozoic transcurrent fault systems with an exposed length of 1,100 km and a width of 350 km, extending in a NW direction across the Arabian Shield into Egypt. Sediments and volcanics conceal some parts of the faults. The system is a braided complex of parallel and curved en echelon faults (Moore et al. 1979).

There are variations in deformational style along this fault system: Strike–slip faulting in the north half of the Shield developed in an environment of higher heat flow and hence was ductile, while the deformation in the crust in the southern half was more brittle (Stern 1985). Individual faults of the Najd system have a maximum left lateral displacement of 65 km in the middle of the Shield (Cole and Hedge 1986), decreasing toward its edges. The system displaced the north trending Al Amar and Nabitah sutures and the northeast trending Bir Umq and Yanbu sutures, resulting in a cumulative displacement of 240 km (Abdelsalam and Stern 1996).

Johnson (1996) distinguished between the NW–SE Najd faults based on their origin time, tectonic implications, and associated structures, and gave them two names: Ar Rika

Fig. 1 Location map showing NFS and general geology

and Ruwah fault zone, respectively (Fig. 2). The Ar Rika fault zone includes the shear zones of Kirsh, An Nakhil, Wajiyah, Hamadat, Ajjaj, and Qazaz gneiss–schist belts and intervening brittle faults. Lineaments interpreted from the aeromagnetic and gravity data suggest an extension of the Najd system beneath the Cover Rocks. These shear zones extend southeast for at least 200 km beneath the Cover Rocks and northwest into Egypt.

The Ruwah fault zone is part of a shorter shear zone that extends to the Zalm area and changes direction to the north, merging with the Ad Dafinah fault. This fault zone continues southeast of the Shield for at least 250 km and continues northwest as the Ash Shakhtaliyah gneiss–schist belt west of Zalm (Johnson 1996).

This study was made to investigate selected sections on the Najd fault system. Therefore, the global position-

ing system (GPS)–gravity survey was primarily designed to provide information about the Najd fault system (NFS) in terms of subsurface geometry. Therefore, ten GPS–gravity profiles were conducted crossing the NFS in two selected areas (Fig. 2), six in the Afif and four in the Al Muwayh area; these are about 500 and 650 km west of Riyadh, respectively. The profiles are 30 km long and 5 km apart. The reading intervals start at 2 km and decrease to about 100 m in the vicinity of the faults. The differential GPS (DGPS) technique employs two receivers that measure and track the same satellites simultaneously. The overall relative height accuracy for Afif and Al Muwayh GPS surveys is within 22 cm. The areas were chosen because each covers a major branch of the NFS, Ar Rika fault zone in Afif area, and Ruwah fault zone in Al Muwayh area.
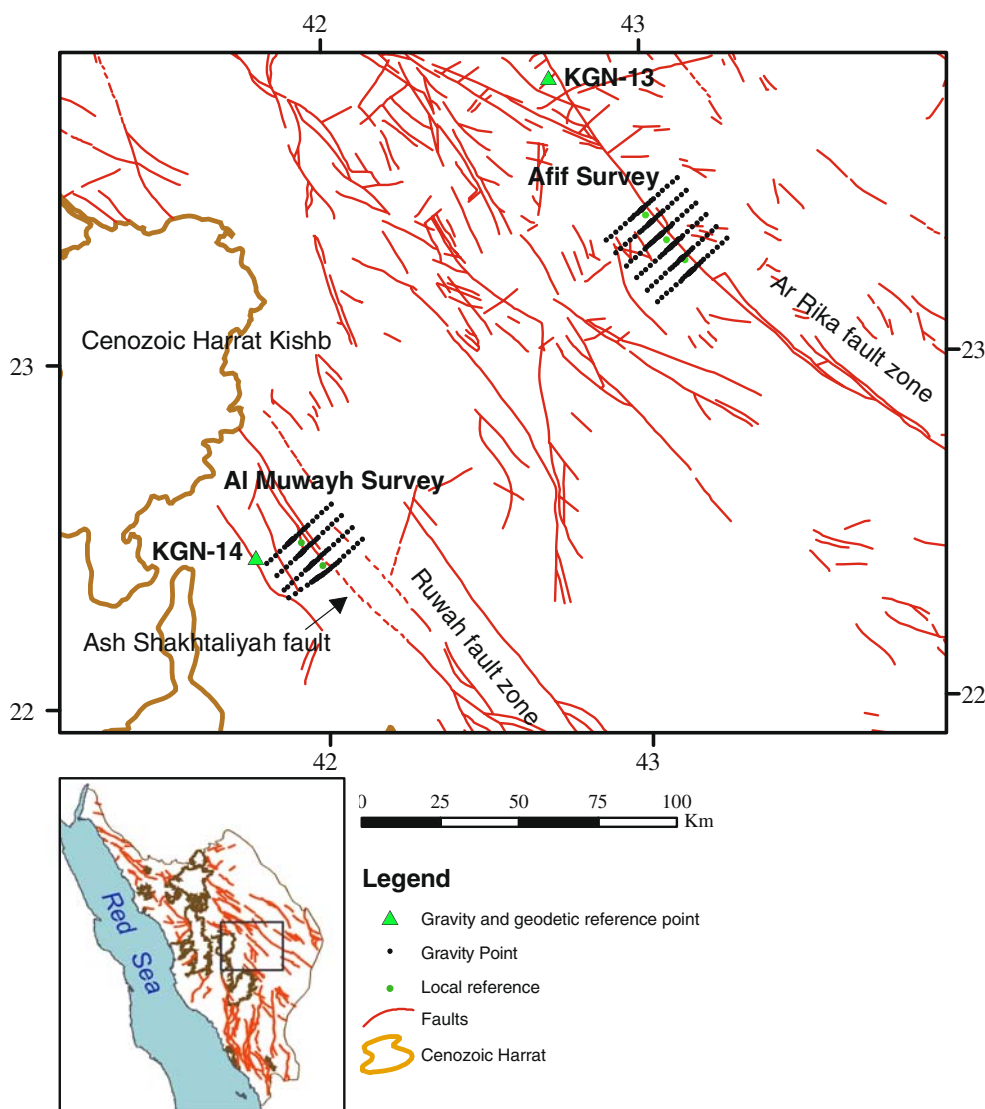
Fig. 2 Location map showing gravity profiles in Afif and Al Muwayh areas superimposed on the general fault lines of NFS
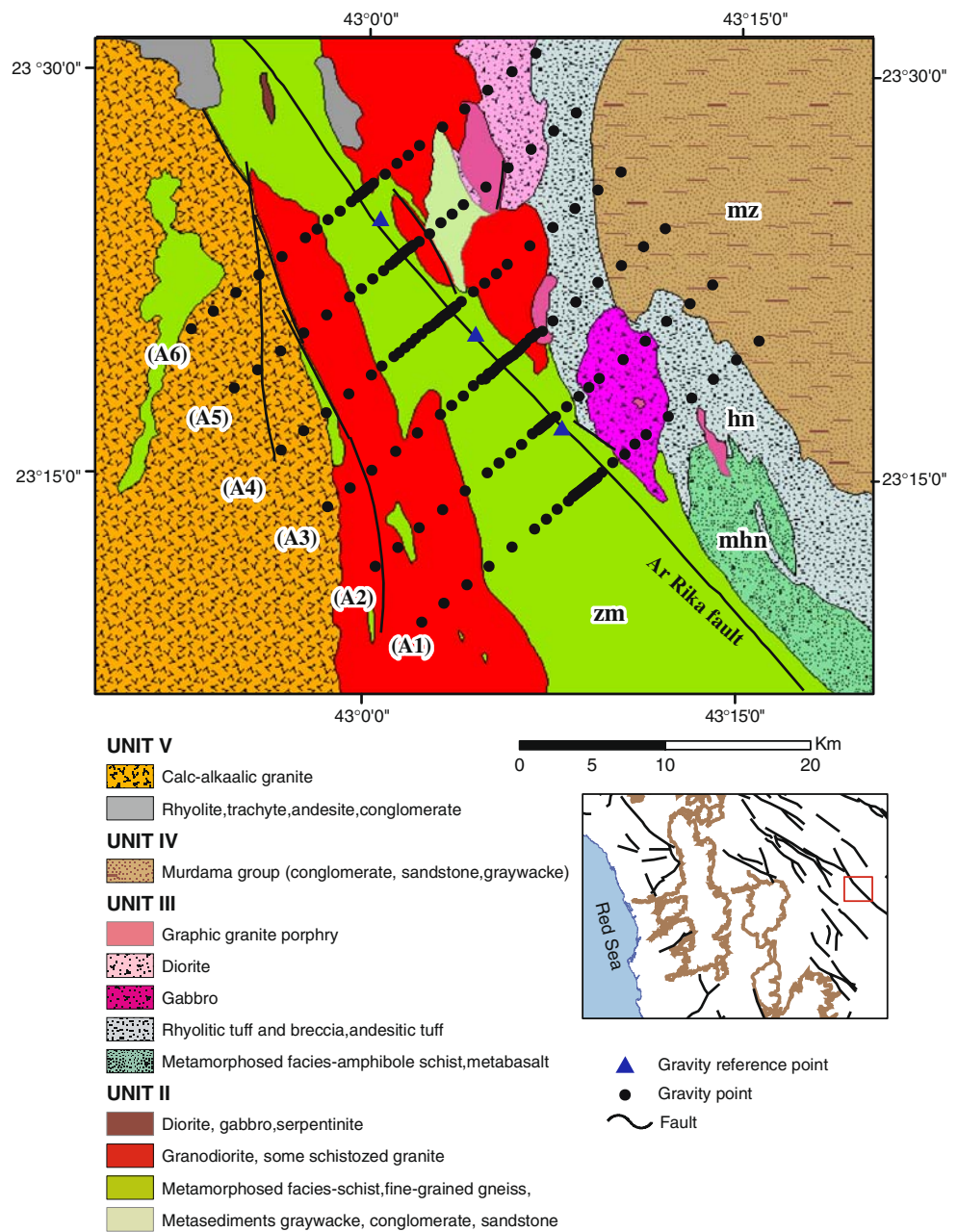
Afif geology

The Afif geological map (Fig. 3) was digitized from the Ministry of Petroleum and Mineral Resources of Saudi Arabia (MPMR) geological maps scale 1:250,000. Digitization was performed by Arcscan™ (extension of ArcGIS™ 9.2). Afif geology map was compiled by Letalenet (1979), as "the Afif quadrangle" that covers an area between latitude 23° and 24° N, and longitude 42° and 43.5° E. According to Letalenet (1979), the Afif quadrangle is almost entirely occupied by five lithostratigraphic units comprising the great Upper Proterozoic tectonic cycle with subsidiary Cambrian sedimentary rock, Tertiary basalt and limestone, and extensive Quaternary surficial deposits. For simplifying the interpretation of the gravity and aeromagnetic data, the surficial deposits were not digitized. The An Nayzah formation as seen in Fig. 3 is a key unit, as it is displaced

by the Ar Rika fault and covered by all gravity profiles of the Afif survey. Part of An Nayzah formation is shown in Fig. 3 as "zm." Another key unit is unit V, which comprises only the alkalic lava of the Shammar group that consists of acid volcanics extruded along the NFS. It overlies the Murdama group. The last phase of the Upper Proterozoic tectonic cycle is represented by postorogenic molasse sediments of the Cambrian age. These sediments produced the Jibalah group, which were deposited in tectonic troughs related to the Najd faults.

Al Muwayh geology

Geological data for the Al Muwayh survey were digitized from two geological maps scale 1:250,000, Zalm quadrangle by Agar (1988) and Al Muwayh quadrangle by Sahl

Fig. 3 Geology map of Afif gravity survey area

UNIT V

Calc-alkaalic granite

Rhyolite,trachyte,andesite,conglomerate

UNIT IV

Murdama group (conglomerate, sandstone,graywacke)

UNIT III

Graphic granite porphry

Diorite

Gabbro

Rhyolitic tuff and breccia,andesitic tuff

Metamorphosed facies-amphibole schist,metabasalt

UNIT II

Diorite, gabbro,serpentinite

Granodiorite, some schistozed granite

Metamorphosed facies-schist,fine-grained gneiss,

Metasediments graywacke, conglomerate, sandstone

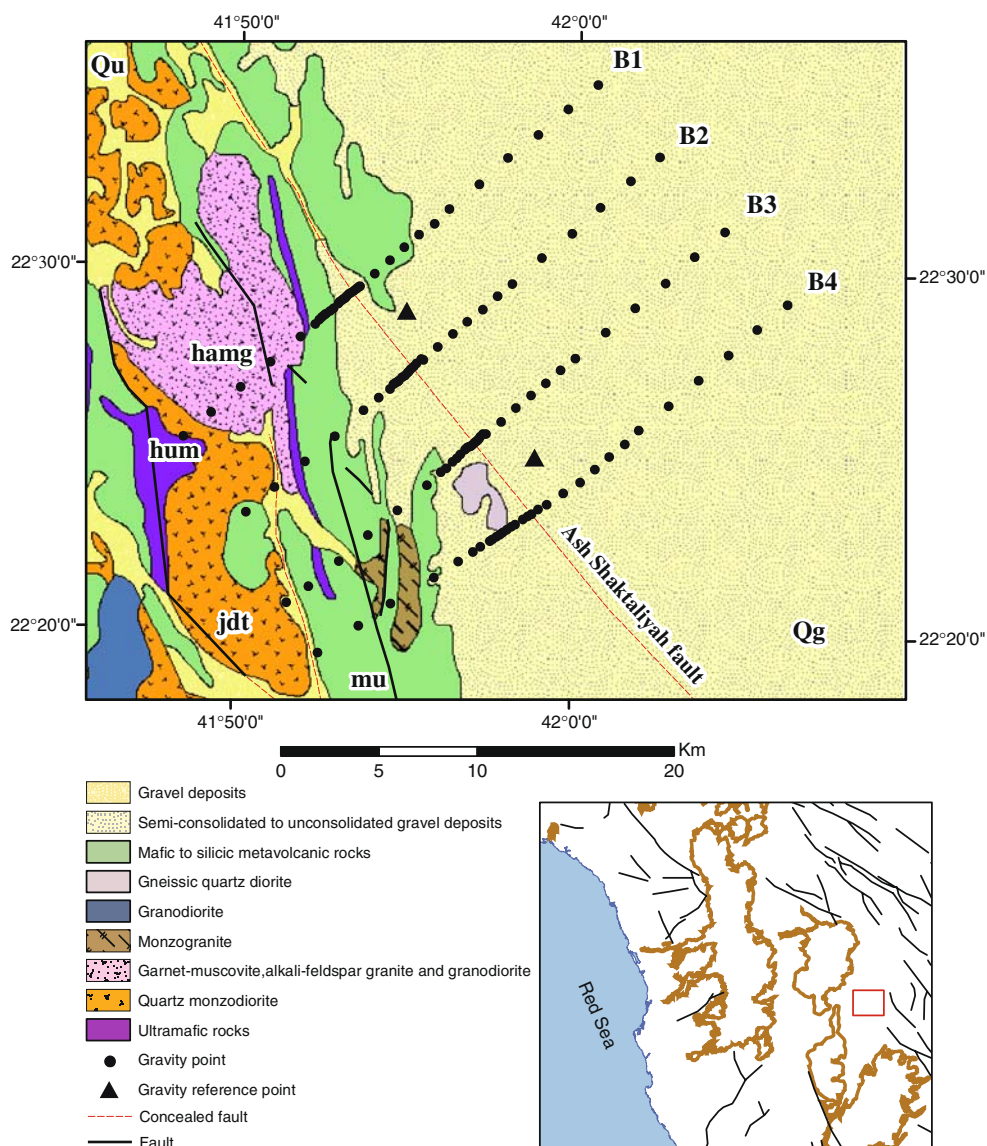▲ Gravity reference point

● Gravity point

⌇ Fault

and Smith (1986). The investigated area is between those quadrangles; the corresponding part from the two maps were scanned and further processed in ERDAS™ 8.6; the processing involved geo referencing and mosaicking into one map, then reprojected to the appropriate projection. The map was exported to the ArcGIS™ 9.2 for further visualizations as seen in Fig. 4. However, it should be mentioned that matching the concealed Ash Shakhtaliyah fault from the two quadrangles showed a shift, which is due to the uncertainty on the location of the fault at Zalm quadrangle as gravel deposits cover it. The main structural feature in the Al Muwayh map (Fig. 4) is the Ash Shakhtaliyah fault, which is a major fault zone representing the western margin of the Najd fault system. The faults trend northwest to

north-northwest with sinistral displacements. An important formation in the area is the Muwayh formation that crops out widely in the west side of the map (Fig. 4) and is the most widespread of the Precambrian stratiform units. The strike of the Muwayh formation was greatly affected by the Najd fault system (Sahl and Smith 1986).

Gravity processing

To tie the GPS–gravity survey to a reference point, for which an absolute gravity reading and geodetic coordinates are available, a search was made for previous work. The only gravity report accessible at the time of the survey was Flanigan

Fig. 4 Geology map of the Al Muwayh gravity survey area

and Akhras ([1972]). The gravity readings of Flanigan and Akhras report were carried out on some geodetic reference points (geodetic network of Saudi Arabia) and later were updated and corrected by the Arabian Geophysical and Surveying Company (ARGAS report V1 [1975]) during their gravity survey. Thus, the plan of these surveys was to connect Afif gravity survey to the absolute-gravity station KGN-13 and Al Muwayh gravity survey to KGN-14 seen in Fig. [2].

Each gravity reading was stored as an attribute to its corresponding GPS reading. The data were exported together with the GPS data to be processed in Microsoft Excel. All gravity data and their accompanying geodetic coordinates were converted to a common set of parameters. These are listed below.

> Latitudes and longitudes reduced to common geodetic reference system "Ain el Abd 1970"

Gravity formula used is the 1967 Geodetic Reference System Formula (GRS67)

$$g_{lat} = 978,031.846(1 + 0.0053024\sin^2(lat) - 0.0000059\sin^2(2 \times lat))$$

The simple Bouguer anomaly was derived using the following formula (SBGA):

$$SBGA = g_{obs} - (g_{lat} - (free\text{-}air\ correction) + (Bouguer\ correction))$$

$$SBGA = g_{obs} - (g_{lat} - 0.3086h + 0.04193\rho h)$$

where g_{obs} is the observed gravity reading, h is the orthometric height in meter, and ρ is the density in grams per cubic centimeter (g/cm^3)

The reduction density used for Bouguer anomalies is 2.67 g/cm^3. Terrain corrections were applied for the gravity surveys using high-resolution digital topographic data provided by the Military Survey Department of Saudi

Arabia, which were used to calculate the terrain corrections. Then, the data were further processed in the Generic Mapping Tools (GMT; Wessel and Smith 1991); terrain corrections were applied in both Afif and Al Muwayh surveys. Gravity data were then visualized in the ArcGIS™.

Gridding

Most interpolation algorithms such as minimum curvature or nearest neighbor perform poorly on data sampled along profiles crossing features whose length scales are small along the profiles but large transverse to them, such as lineaments. Rather than reproducing the linear features, these algorithms create a series of closures around the profiles. Therefore, the gravity data were gridded by triangulations (Shewchuk 2002). This kind of gridding performs directly or indirectly Delaunay optimal triangulation of arbitrarily spaced (x, y, z) data. To avoid sharp angles resulting from uneven data distribution, the girds were gridded at 0.0005° and filtered by cosine filter to smooth high angles in the produced grids. Delaunay triangulation interpolates the data to form $z(x, y)$ as a union of planar triangular surfaces. One advantage of this method is that it will not extrapolate $z(x, y)$ beyond the
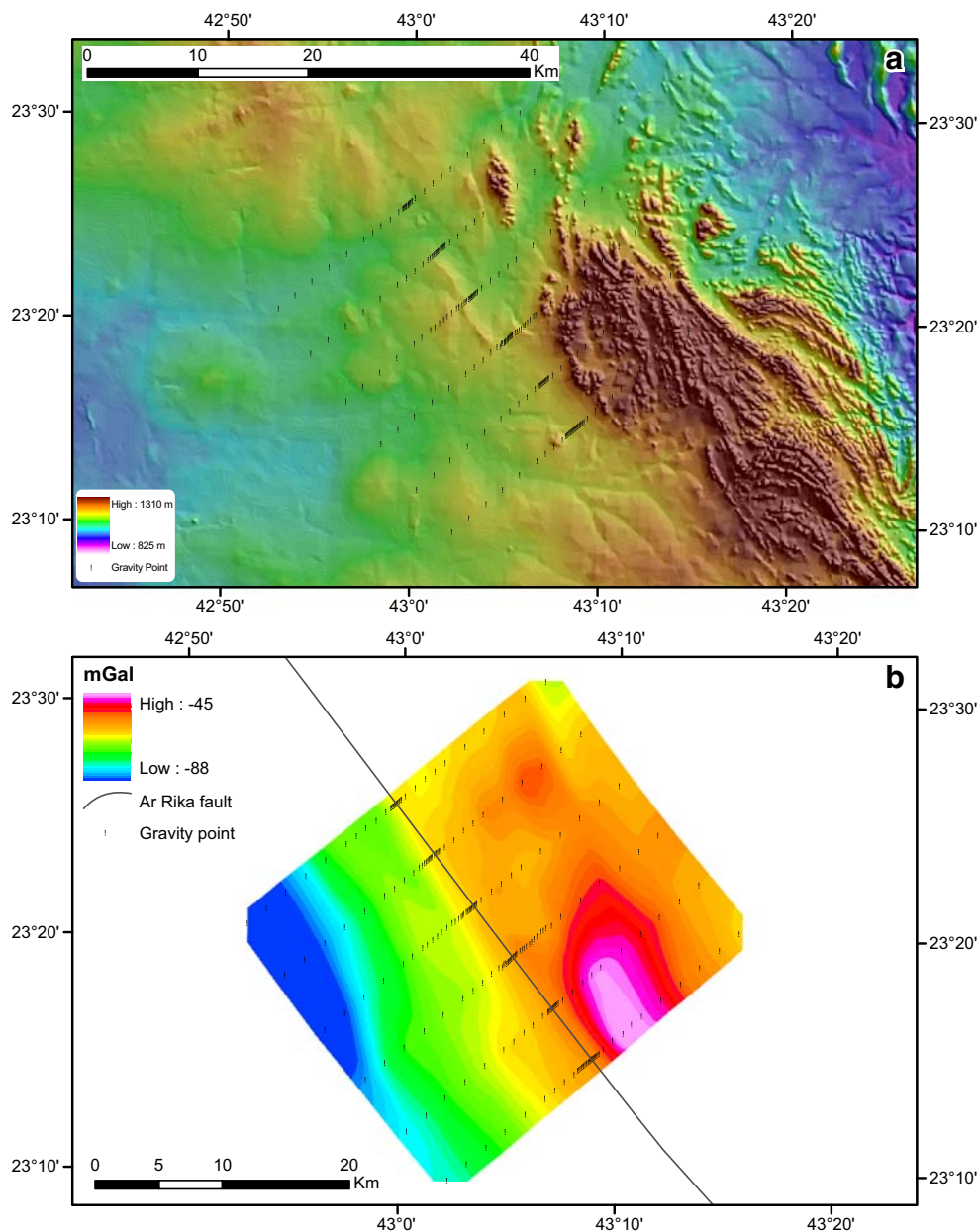

Fig. 5 **a** and **b** Topography and Bouguer anomaly maps of Afif survey, respectively

convex hull of the input (x, y) data. Another is that it will not estimate a z value above or below the local bounds on any triangle. A disadvantage is that the z(x, y) surface has sharp kinks at triangle edges and thus also along contours. This may not look physically reasonable, and therefore, the resultant grids were filtered prior to visualization.

Isostatic residual anomaly

The Bouguer anomaly map images anomalies that result from the whole crustal section including variations in the Moho and lateral densities in the upper mantle. The long-wavelength gradients seen in Figs. 5b and 6b could result from variations in Moho thickness and tend to obscure the upper crustal structures that are related to the faults. These long-wavelength Bouguer anomalies can be estimated in the form of the isostatic correction and removed from the Bouguer anomalies (Watts 2001).

Isostatic residual anomaly = Bouguer anomaly

− isostatic correction

The isostatic correction accounts for assumed variations in the depth of the Moho. For much of Saudi Arabia, in
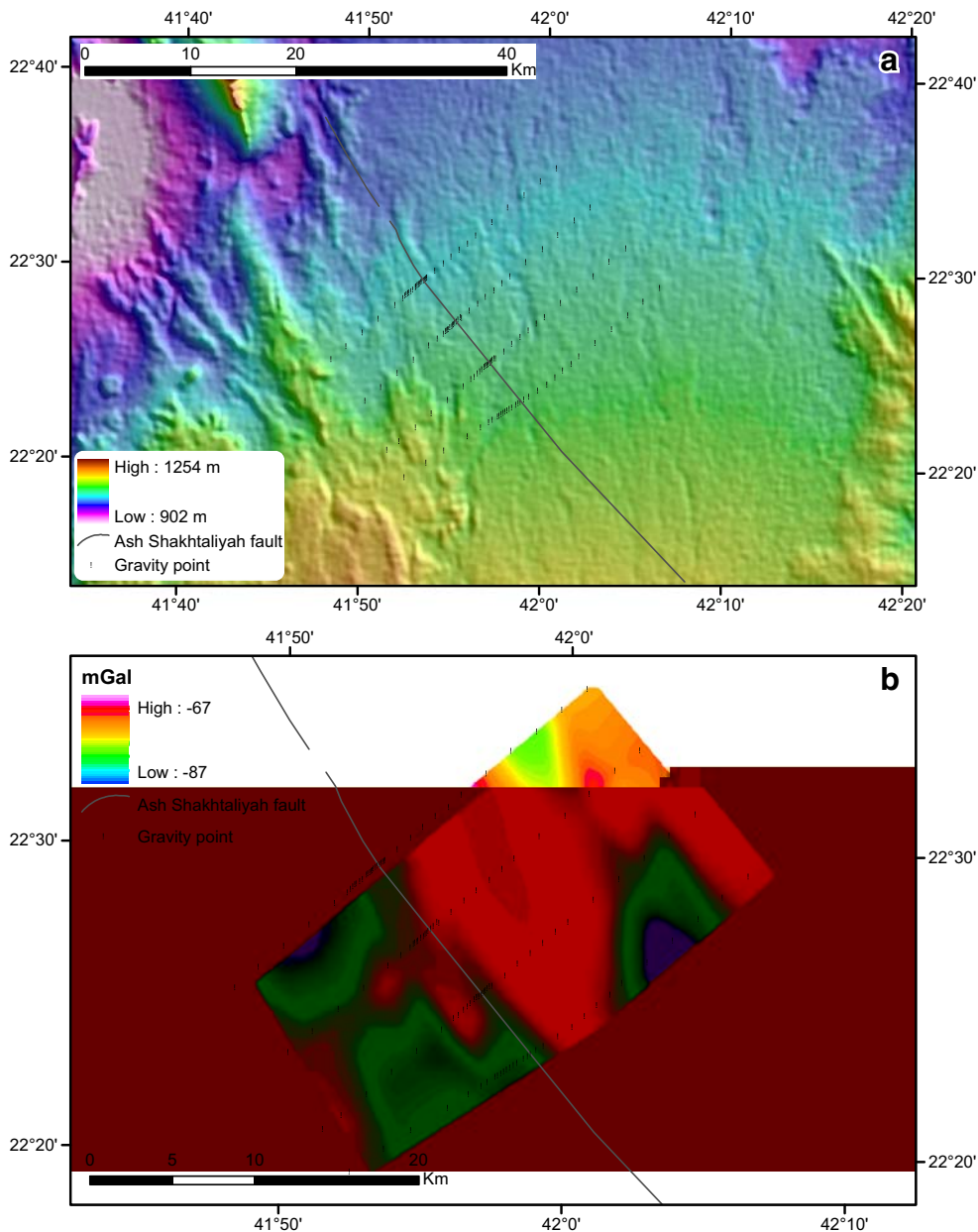

Fig. 6 a and b Topography and Bouguer anomaly maps of Al Muwayh survey, respectively

particular the Arabian Shield, one can assume that a simple system of isostatic equilibrium is operating. This assumption implies a simple relation between topographic relief and the Moho depth.

The Airy–Heiskanen model of isostacy has been used in this study to derive the isostatic correction. The Airy–Heiskanen model assumes a fixed density for the crust and varying depth of the Moho to compensate for the mass of the topography. To remove the effect of the compensating masses beneath the topography highs, Airy isostasy has been assumed. The gravitational attraction of the Moho was determined from the 30-arcsecond topography data. Calculation of the isostatic correction field was performed using the grid-based fast Fourier transform accompanied by the geophysical software program GMT 3.4.4 (Wessel and Smith 1991), using 2.67 and 3.3 g/cm^{-3} densities for the crust and mantle, respectively. A mean thickness of 40 km was used, which is the mean thickness of the crust in Saudi Arabia (Al-Amri 1999; Badri 1991; Levin and Park 2000; Al-Damegh et al. 2005). Calculation procedures and parameters were modified with the help of Dr. Walter Smith (personal communication). The isostatic correction field shown was subtracted from the observed Bouguer anomaly to produce the isostatic residual anomaly.

The isostatic residual map better images short-wavelength structures within the upper crust that are of interest in this study. However, the continued presence of long-wavelength anomalies in the isostatic residual map indicates that the region containing the study area is either not in isostatic equilibrium or assumptions used in the determination of the isostatic correction are not entirely valid (e.g., the crust is not responding in an Airy manner with effect elastic thickness, Te=0), or there are density variations in the upper mantle. The isostatic residual anomaly has been further corrected by the decompensative correction discussed in "Decompensative isostatic residual anomaly."

Decompensative isostatic residual anomaly

Decompensative anomalies are mainly produced by density inhomogeneities in the upper 15–20 km of the crust (Cordell et al. 1991). The isostatic correction has eliminated the gravity-compensating effect of topography but other long-wavelength gravity effects due to features not accounted for in the Airy model remain.

Lockwood (2004) has discussed the concept of bottom loading of Forsyth (1985) and suggests that variations in the depth to the base of the crust could be caused by processes originating in the mantle and that some of the topography of the crust could be, in part, the response of a load applied at the base of the crust.

The decompensative correction attempts to remove the anomalies associated with sources deeper than the crust. These gravity effects are isolated by upward continuation. Therefore, the isostatic residual anomaly has been upward continued to 40 km so that the resulting field due to sources at or deeper than 40 km can be estimated. The decompensative gravity anomaly field as shown in Figs. 7a, 8a, and 9a was determined by subtracting the upward continued field from the isostatic residual anomalies.

Lockwood (2004) argued that the results of the separation filtering process by upward continuation of the potential field should be interpreted qualitatively rather than quantitatively due to the fact that it is impossible to guarantee that the upward continued field contains only signals from the deeper sources.

The resultant decompensative anomalies can be assumed to be produced mainly by density inhomogeneities in the upper 15–20 km of the crust. Thus, Figs. 7b, 8b, and 9a should closely correlate with the major geological structures in the study area. The resultant decompensative gravity data has been used with aeromagnetic data for interpreting the structures of the Ar Rika and Ruwah.
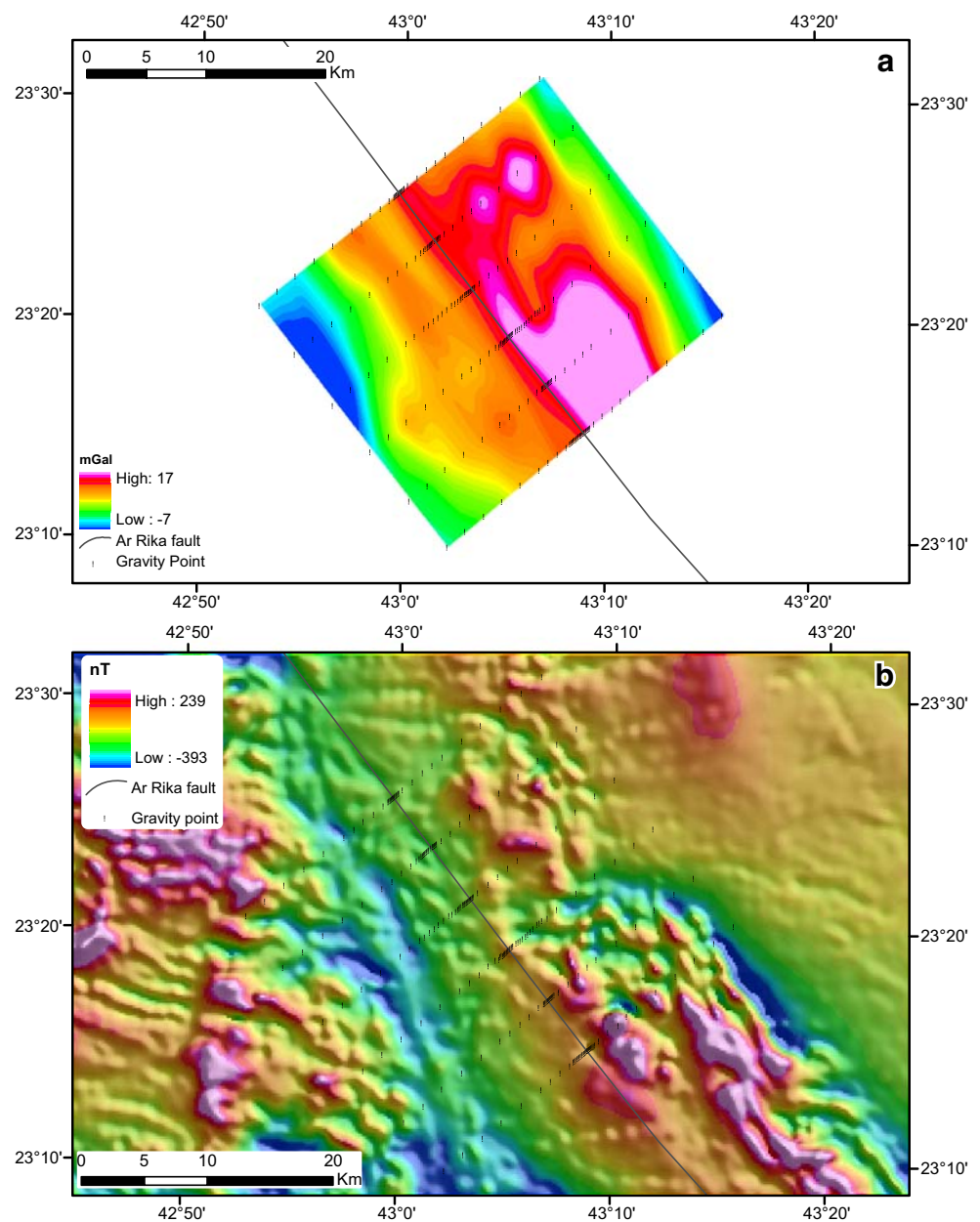
Magnetic and gravity characteristics

Aeromagnetic and gravity data were carefully processed to enhance detailed geological features. Total magnetic intensity and reduced to pole (RTP) and their derivatives (tilt and first vertical) plus the decompensative isostatic residual gravity (DI) data were integrated with the geology maps and in GIS (ArcGIS™) software for fast and better correlations. Quantitative interpretations of selected anomalies were performed by modeling seen in Figs. 10 and 11.

In general, the aeromagnetic data proved a good tool for mapping the internal structures of the terranes, whereas gravity proved effective 'where data coverage permits' in delineating the deeper structures such as distribution of continental masses and molasse basins.

Ar Rika faults

Close correlation between the Ar Rika fault and the Bouguer anomalies is evident (Fig. 5b); however, the decompensative isostatic residual map (Fig. 7a) better images the Ar Rika fault as long-wavelength anomalies were removed. Ar Rika faults zone trends in NW–SE direction (about S 130° E), and in its southern parts, it shows weak aeromagnetic signatures due to the lower susceptibility rock types of the fault zone (phyllite and meta-conglomerate of the Murdama group, and some

Fig. 7 **a** and **b** Decompensative isostatic residual anomaly map and total intensity aeromagnetic map of Afif survey, respectively
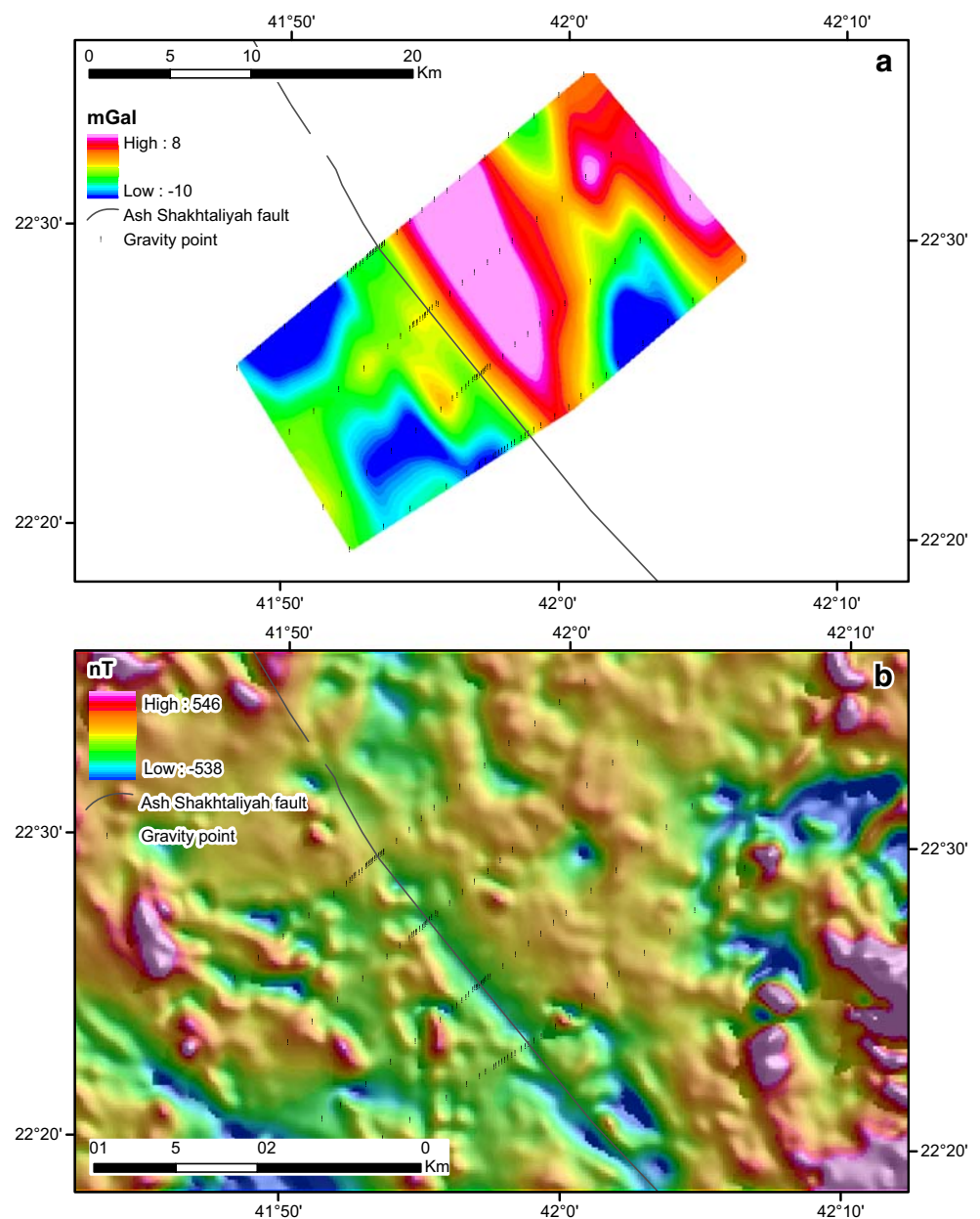

granite gneiss and amphibolite). Aeromagnetic anomalies associated with this fault zone range from 50 to 100 nT in the southern part and about 150 nT east of the gneiss dome at approximately 44° E and 23° N. In the area near the location 44.15° E and 22.65° N, the gneiss belt of the Ar Rika fault zone splays into two parts. The Ar Rika fault zone is characterized by broad positive gravity anomalies (20–30 mGal) in the decompensative isostatic residual gravity map (Fig. 9), which might be a response to deeply-lying higher density gneiss. Geometry of the subsurface structure of Ar Rika fault is modeled (Fig. 11) as an inclined fault with reverse movement, which would imply a compression component (post-dated the shearing) parallel to the plane of the cross-section.

Ruwah faults

The Ruwah faults zone, which is considered by Johnson and Kattan (2001) as a suture zone, trends in the NW–SW direction (about 130°) and is about 15 km wide associated with gneiss domes. The decompensative isostatic residual map (Fig. 8a) shows an obvious gradient that correlates with the Ash Shakhtaliyah fault (which is part of Ruwah faults). These correlation and anomalies to the east of the fault may be caused by deeper sources. Ash Shakhtaliyah fault is also associated with clear negative magnetic anomalies as seen in Fig. 8b.

The Ruwah fault zone is characterized by several narrow, very strong short-wavelength elongated magnetic

Fig. 8 **a** and **b** Decompensative
isostatic residual anomaly map
and total intensity aeromagnetic
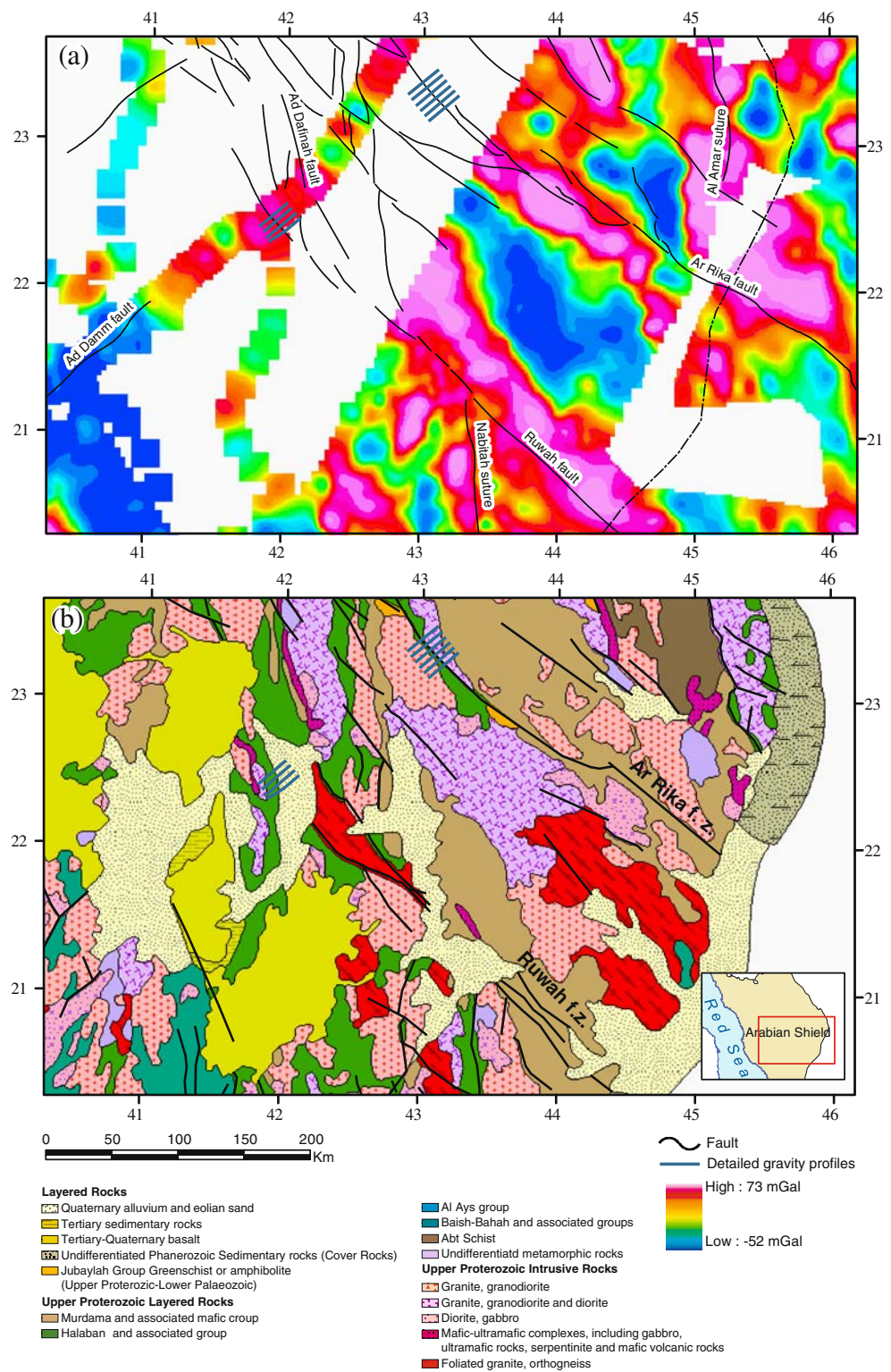map of Al Muwayh survey,
respectively

anomalies (Fig. 12), ranging in amplitude from 100–150 nT
in the southern part of the fault zone to 200–300 nT in the
northern part of the zone. To the west of the Ruwah fault
zone (at approximately 43.4° E and 21.3° N) lies the N–S
trending dextral strike–slip Nabitah suture, which is marked
by strong negative short-wavelength magnetic anomalies
ranging from −200 to −400 nT.

The Ruwah zone also truncates and drags anomalies
of the Nabitah suture zone so that these structures
become part of the Ruwah zone. Further north about
42° E and 22.5° N, the Ruwah faults splay into the N–S
Nabitah suture referred to as the Ad Dafinah fault.
Aeromagnetic data show major sigmoidal shape anoma-
lies between the Najd shears and are usually the result
of dragging of the N–S Nabitah along the Najd shears

and translations along minor shears between them.
Quaternary gravel concealed most of the critical region
where the Ruwah and Ad Dafinah fault zones meet;
however, continuity is clearly shown between the fault
zones by the curved lineaments of high-amplitude short-
wavelength magnetic anomalies.

Decompensative isostatic residual gravity map (Fig. 9)
shows broad positive anomalies (about 20 mGal) to the east
of the Ruwah fault zone, which is probably due to the
gneiss dome associated with the shear. Modeling the
gravity field crossing the Ruwah fault zone (Fig. 9)
revealed that it is associated with low-gravity anomalies
probably due to a complex of lower density crushed rocks.
Structures of the Nabitah suture appear as positive gravity
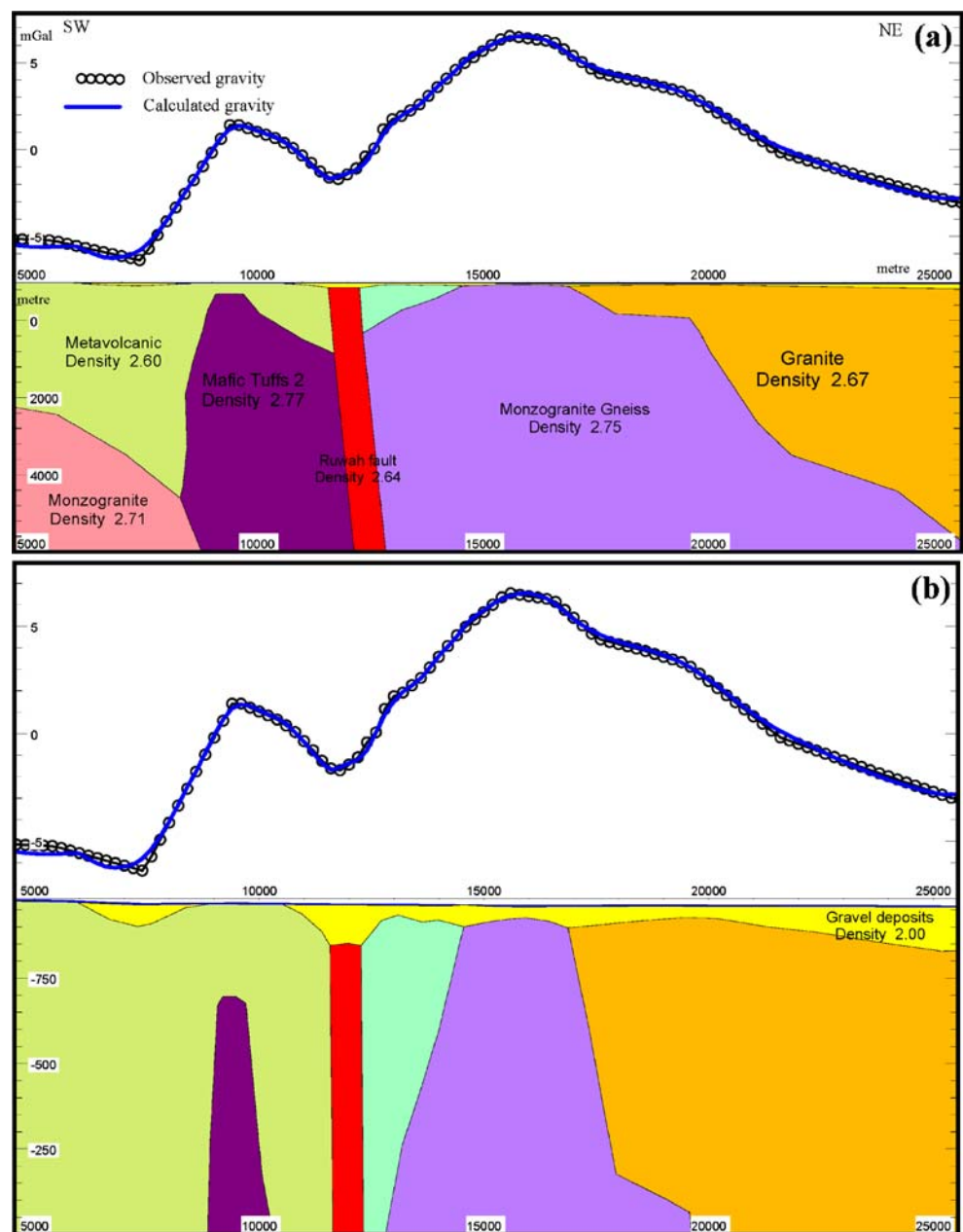anomalies about 20 km in width and 200 km length.

Fig. 9 Colour map of the decompensative isostatic residual gravity (**a**) and its correspondence geological map (**b**) for the Ruwah and Ar Rika shear zones

The decompensative isostatic residual gravity map shows a prominent gravity low (about 30 mGal) between two strands of Najd fault system, Ruwah and Ar Rika faults, coinciding with the Khida crust. Within the Khida crust, some shear faults of WNW–ESE direction with horizontal displacements of about 3 km are evident and

might be a product of a different stage of the Najd faulting. These shears might have been rotated with the Khida crust during the shearing along the Ar Rika fault zone. However, dyke swarms along the said trend might be explained as the product of an extensional system associated with the Najd shearing that, at some stage, was associated with shearing.

Fig. 10 a Gravity modeling from the new detailed gravity survey of Al Muwayh Area, crossing Ash Shakhtaliyah fault (part of Ruwah fault). **b** Vertically exaggerated shallow view. Location of this model is shown in Fig. 12

Both the Ruwah and Ar Rika faults are slightly disrupted by faint long E–W trending anomalies that were enhanced using the first vertical derivative (FVD).

Aeromagnetic maps show sub-parallel N–S wide negative anomalies between the Ruwah and Ar Rika faults. These anomalies are truncated and displaced by the NW–SE faults and coincide with major molasse basins of that region (Murdama and Abt basins).
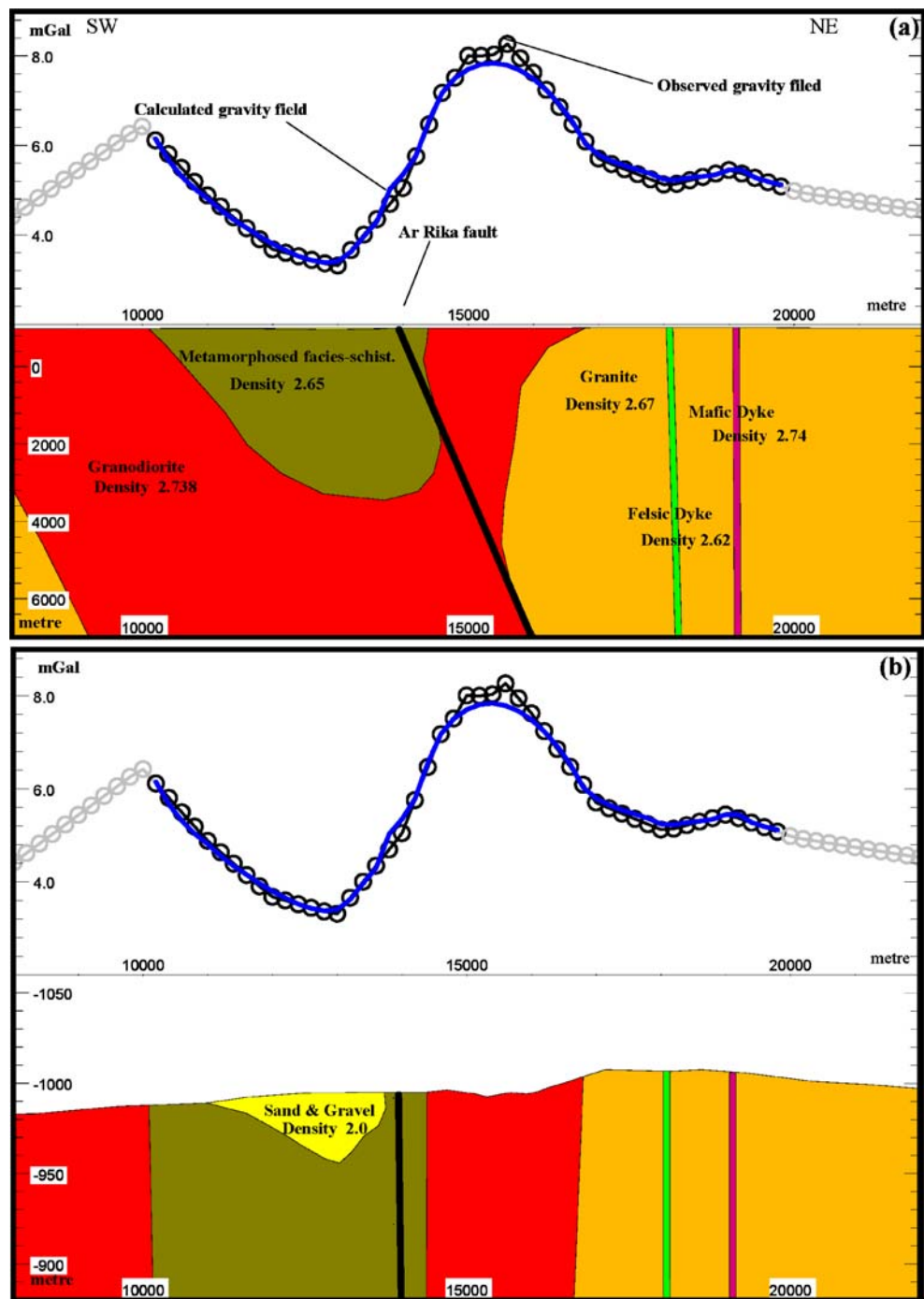
N–S magnetic anomalies associated with the Ad Dafinah–Hulayfah fault zone are truncated because they are offset by the faults of the Najd fault system (the Ar Rika and Halaban–Zarghat fault zone). The N–S Ad Dafinah fault zone passes into the Ruwah NW–SE fault zone toward the south, and hence, this trend is considered a suture by Johnson and Kattan (2001). In the southern part of the Shield, Johnson and Kattan (op cit) considered the Ruwah fault zone as a boundary that separates the Khida crust from the accretionary terrane of the Asir. The zone is characterized by strong short-wavelength, north-trending magnetic anomalies due to the presence of high susceptibility serpentinites and other mafic bodies along the zone.

Conclusions

The use of potential field, geological data, integrated within a GIS (ArcGIS)™ environment, has helped to obtain a

Fig. 11 a Gravity modeling from the new detailed gravity survey of Afif area, crossing Ar Rika faults. **b** Vertically exaggerated shallow view. Location of this model is shown in Fig. 12; note that points shown in *gray* are not calculated
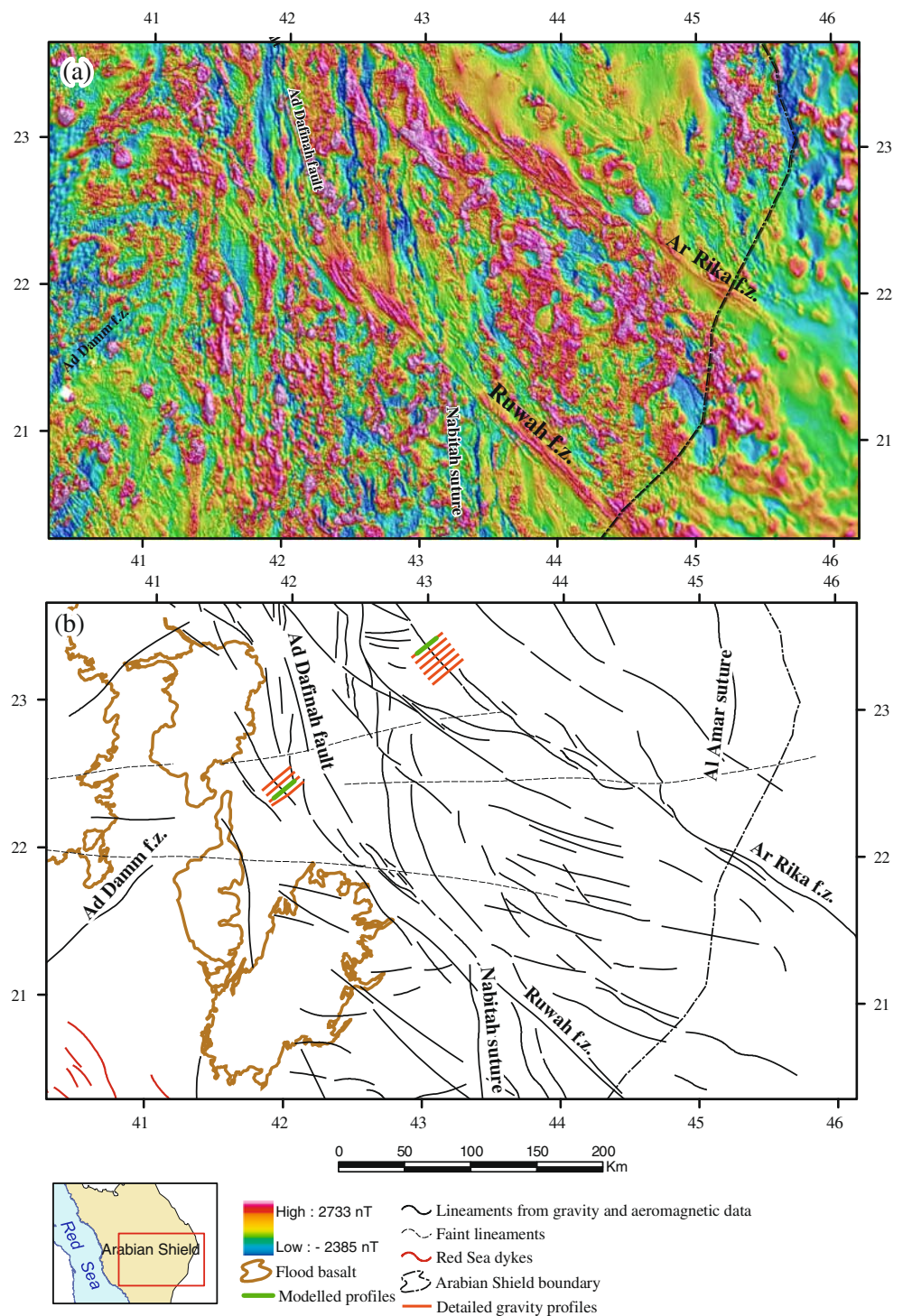

better understanding of the development and structure the Ar Rika and Ruwah faults.

This paper shows that the isostatic residual anomaly attempts to isolate the gravitational effects of the geology contained within the upper crust. It is often calculated using a simple 'Airy' model of isostasy that assumes a zero crustal strength, constant density crust and mantle, and a simple relationship between topographic height and Moho depth. Although the corrections for the variations in Moho

depth work well when the other assumptions are valid, it often fails, although it is not necessarily obvious where. The decompensative anomaly is the difference between the isostatic residual anomaly and its upward continued field at 40 km. The decompensative anomaly thus images all anomalies with wavelengths less than or about 70 km, while the upward continued field identifies the spatial set of anomalies greater than 70 km where the isostatic assumptions may be invalid. Please note that the words may be

Fig. 12 *Color-shaded* RTP
aeromagnetic map (**a**) and its
interpretation (**b**); shown are
distributions of the Ruwah and
the Ar Rika shear zones

invalid because it is possible to have upper crustal
geological features that generate wavelengths in excess of
70 km. These anomaly types can thus help in the analysis
of the spatial changes seen in the surface geology.

The two major shear zones Ar Rika and Ruwah within
the Shield are separated by relatively less-deformed areas

that contain NW–SE translation planes along which
bending of the N–S Nabitah structures is obvious. Geom-
etry of the subsurface structure of Ar Rika fault is modeled
as an inclined fault with reverse movement, which would
imply a compression component (post-dated the shearing)
parallel to the plane of the cross-section.

References

Abdelsalam MG, Stern RJ (1996) Sutures and shear zones in the Arabian–Nubian Shield. J Afr Earth Sci 23:289–310

Agar RA (1988) Geologic map of the Zalm quadrangle, sheet 22F, Kingdom of Saudi Arabia Saudi Arabian Deputy Ministry For Mineral Resources, Jeddah, Saudi Arabia

Al-Amri AMS (1999) The crustal and upper-mantle structure of the interior Arabian Platform. Geophys J Int 136:421–430

Al-Damegh K, Sandvol E, Barazangi M (2005) Crustal structure of the Arabian plate: new constraints from the analysis of tele-seismic receiver function. EPSL 231:177–196

ARGAS report V1 (1975) Gravity survey in Saudi Arabia Ministry of Petroleum and Mineral Resources, Aerial Survey Department, Riyadh, Saudi Arabia

Badri M (1991) Crustal structure of central Saudi Arabia determined from seismic refraction profiling. Tectonophysics 185:357–374

Cole JC, Hedge CE (1986) Geochronologic investigation of Late Proterozoic rocks in the northeastern Shield of Saudi Arabia: Deputy Ministry for Mineral Resources, Technical Record USGS-TR-05-5, Scale 1:1,000,000, 42 p

Cordell L, Zorin YA, Keller GR (1991) The decompensative gravity anomaly and deep structure of the region of the Rio Grande rift. J Geophys Res 96:6557–6568

Flanigan VJ, Akhras MN (1972) Preliminary Report on the Gravity Net in Saudi Arabia, Kingdom of Saudi Arabia Ministry of Petroleum and Mineral Resources, Directorate General of Mineral Resources, Jeddah, Saudi Arabia

Forsyth DW (1985) Subsurface loading and estimates of the flexural rigidity of continental lithosphere. J Geophys Res 90:12623–12632

Johnson PR (1996) Geochronologic and isotopic data for rocks in the East-Central part of the Arabian Shield Stratigraphic and Tectonic Implications Ministry of Petroleum and Mineral Resources, Directorate General of Mineral Resources, Jeddah, Saudi Arabia

Johnson PR, Kattan F (2001) Oblique sinistral transgression in the Arabian shield: the timing and kinematics of a Neoproterozoic suture zone. Precambrian Res 107:117–138

Letalenet J (1979) Geologic map of the Afif quadrangle, sheet 23F, Kingdom of Saudi Arabia Saudi Arabian Deputy Ministry For Mineral Resources, Jeddah, Saudi Arabia

Levin V, Park J (2000) Shear zones in the Proterozoic lithosphere of the Arabian Shield and the nature of the Hales discontinuity. Tectonophysics 323:131–148

Lockwood A (2004) Isostatic and decompensative gravity anomalies over Western Australia. Australian Society of Exploration Geophysicists, Preview 108:22–23

Moore JM, Allen P, Wells MK, Howland AF (1979) Tectonics of the Najd transcurrent fault system, Saudi Arabia. Journal of the Geological Society of London 136:441–454

Sahl M, Smith JW (1986) Geologic map of the Al Muwayh quadrangle, sheet 22E, Kingdom of Saudi Arabia Saudi Arabian Deputy Ministry For Mineral Resources, Jeddah, Saudi Arabia

Shewchuk JR (2002) Delaunay refinement algorithms for triangular mesh generation. Computational Geometry, Theory and Applications 22:21–74

Stern RJ (1985) The Najd Fault System, Saudi Arabia and Egypt—a late Precambrian rift-related transform system. Tectonics 4:497–511

Watts AB (2001) Isostasy and flexure of the lithosphere. Cambridge University Press, Cambridge

Wessel P, Smith WHF (1991) Free software helps map and display data: EOS Trans. AGU 72:445–446